A Method of Seamless Transitions Between Different Operating Modes for Three-Port DC-DC Converters

HAMZEH ALJARAJREH[1], **(Member, IEEE), DYLAN DAH-CHUAN LU**[1], **(Senior Member, IEEE), YAM P. SIWAKOTI**[1], **(Senior Member, IEEE), RICARDO P. AGUILERA**[1], **(Member, IEEE), AND CHI K. TSE**[2], **(Fellow, IEEE)**

[1]School of Electrical and Data Engineering, University of Technology Sydney, Sydney, NSW 2007, Australia
[2]Department of Electronic and Information Engineering, The Hong Kong Polytechnic University, Hong Kong

Corresponding author: Hamzeh Aljarajreh (hamzeh.aljarajreh@ieee.org)

ABSTRACT This paper presents the design of three-port converters (TPCs) for smooth transitions (i.e., fast settling time, and no obvious overshoot/undershoot) of 7 distinctive operating modes, depending on sources and loads scheduling. Two viable converter configurations have been identified and selected for further analysis and design of PV-battery systems. Conventionally, mode transition is achieved by assigning specific switching patterns through feedback signals and appropriate control algorithms. This incurs a delay in the response and unavoidable noise in the circuit. Additionally, in TPCs, three voltage sensors and three current sensors are generally required for decision making in mode selection, where errors in sensors may lead to an inaccurate response. This paper presents a new control strategy where the number of switching patterns is significantly reduced to 3 patterns instead of minimum 5 patterns for existing reported topologies. Therefore, decisions are simplified so that the transition occurs naturally based on the power availability and load demand but not deliberately as in the conventional method. In addition, instead of six sensors, three voltage sensors and only one current sensor are required to achieve all the necessary operations, namely, MPPT, battery protection, and output regulation. Moreover, these sensors do not participate in mode selection decision, which leads to seamless and fast mode transition. In addition, this work considers two bidirectional ports as compared with only one bidirectional port in most reported topologies. This configuration enables both standalone and DC grid-connected applications. Experimental results are reported to verify the proposed solution.

INDEX TERMS Auto-transition, battery, bidirectional converter, mode selection, photovoltaic system and three-port converter.

I. INTRODUCTION

For hybrid energy systems, it is accustomed to use multiple single-input single-output (SISO) converters to connect different sources and loads. However, it is potentially bulky, high cost and less efficient. Therefore, multiple-input single-output (MISO) converters, on the contrary, are capable of converting power from multiple power sources to the load individually or simultaneously by using simplified circuitry and appropriate control strategy. Three-port power

converters (TPCs) are widely employed in various applications such as electric vehicles [1]–[3], photovoltaic hybrid systems [4], and fuel-cell hybrid power systems [5]. Three-port converters may consist of a unidirectional port such as PV source or a bi-directional port such as battery [6]–[8]. Therefore, the arrangement of converters and controller for the power flow distribution in a TPC plays a vital role on the overall performance and efficiency. Recently, a systematic analytical technique for different configurations has been proposed [9]–[11]. However, for some applications such as electric vehicles, a bidirectional output port is required to handle regenerative braking [12], [13]. All possible power

The associate editor coordinating the review of this manuscript and approving it for publication was N. Prabaharan.

H. Aljarajreh *et al.*: Method of Seamless Transitions Between Different Operating Modes for Three-Port DC-DC Converters

IEEE *Access*

flow combinations for two bidirectional ports have been constructed previously [14], which cover cases with all ports fully or partially controlled as well as selected configuration for specific applications. Each power flow graph is a combination of power flow subgraphs. There are three types of power flow subgraphs: (1) Type I, which transfers power separately from one port to another port, (2) Type II, which transfers power simultaneously from two ports to one port, (3) Type III, which transfers power simultaneously from one port to two ports. This study focuses on two of the most appropriate power flow configurations, namely, Type II-IIA and Type II-IIB. These configurations offer a single-stage converter to increase the efficiency and a full control of the ports.

Many three-port converters with a unidirectional output port have been presented previously [15]–[18]. However, the scenarios where power transfer from PV to load only and PV to battery only have not been considered. In addition, the battery protection condition is not well defined. This problem was later addressed in [19]–[21], but three current sensors and three voltage sensors are employed to compare the power from each port.

Most of the reported works aim to achieve Maximum Power Point Tracking (MPPT), battery voltage regulation and output voltage regulation. However, not all control objectives are achieved simultaneously [22], [23]. Although it is integrated and has single power processing feature for all ports, the control dimension is inevitably limited. In addition, the PV to load transfer mode cannot be activated without physically disconnecting the battery [24]. Other three-port converters are presented in [25] and [26], where the battery regulation is achieved by estimating the state-of-charge from the terminal voltage, and mode transition is activated and restricted to only after a specific period of time. In [27], the transition between modes occurs after a delay of 0.3 s and the PV array is emulated by dc voltage source. In [28] & [29], three-port bidirectional DC/DC converters are proposed with new control strategy. However, transition between modes is not considered. A two-stage solar PV based three-port converter is proposed in [30]. This converter has a balanced control in selecting between MPPT and battery voltage regulation. However, it does not allow for no load and full PV power scenarios. There is also an overshoot and a delay in the transition between modes. Three-port converters with two bidirectional ports is presented in [31], [32]. However, mode transition is achieved by assigning specific switching patterns periodically, which causes a delay in the response and unavoidable noise in the circuit. Also, the errors in sensors may lead to inaccurate response.

Based on Table 4 and motivated by all these challenges, this paper presents two typical three-port converters with two bidirectional ports and a simple switching pattern control for all the switches so that the system can move from one mode to another according to the power of each port. MPPT, output voltage regulation and battery voltage regulation can be achieved simultaneously. The following advantages are summarizing the contributions of this work:

- Only 4 sensors are used as compared to 6 sensors in the conventional method.
- Only two selection conditions are used as compared to 4 or 5 with prior works.
- This work considers two bidirectional ports as compared with only one bidirectional port in most reported topologies. This enables both standalone and DC grid-connected applications.
- 7 modes of operation with seamless and smooth transition between mode is achieved.
- Fast response where maximum settling time is 100ms or less.

The paper is organized as follows: In Section II, the circuit design, principles of operation and working conditions of Type II-IIA and Type II-IIB configurations are studied. In Section III, the control structure and mode selection are explained. In Section IV, the experimental setup and measured waveforms are presented, followed by conclusion in Section V.

II. OPERATION OF TYPES II-IIA AND II-IIB CONVERTERS

This section discusses the circuit operation of Type II-IIA and Type II-IIB converters, which is applied to a PV-battery powered DC system. In these circuits, a PV source is connected to a unidirectional input port, whereas the battery and DC bus are connected to bidirectional ports. In the Type II-IIA converter, the first converter that connects the PV to the DC bus is a bidirectional buck-boost converter and the second converter is a bidirectional buck-boost converter connecting the PV to the battery, as shown in Fig. 1(a). In the Type II-IIB converter, the first converter that connects the PV to the DC bus is a synchronous buck converter and the second converter is a bidirectional buck-boost converter connecting the battery to the DC bus as shown in Fig. 1(b). The principle of operation of all modes is first studied, followed by a steady state analysis. The converters are assumed to operate in continuous conduction mode (CCM).

A. PRINCIPLES OF OPERATION AND MODES ANALYSIS

The presented three-port converter has seven modes of operation. These modes are discussed in detail as below:

1) **PV to DC bus:** This mode is activated when the PV power supplies the DC bus only as the battery is fully charged or preset maximum State of Charge (SoC).
2) **PV to battery:** This mode is activated when the battery is charged by the PV source at no load condition.
3) **PV to DC bus and battery:** This mode is activated when the PV has sufficient power to supply the DC bus and the battery. The system now operates as a single-input double-output (SIDO) converter.
4) **PV and battery to DC bus:** This mode is activated when the DC bus requires more power than the PV source can generate. Therefore, the battery should provide the remaining power to the DC bus.
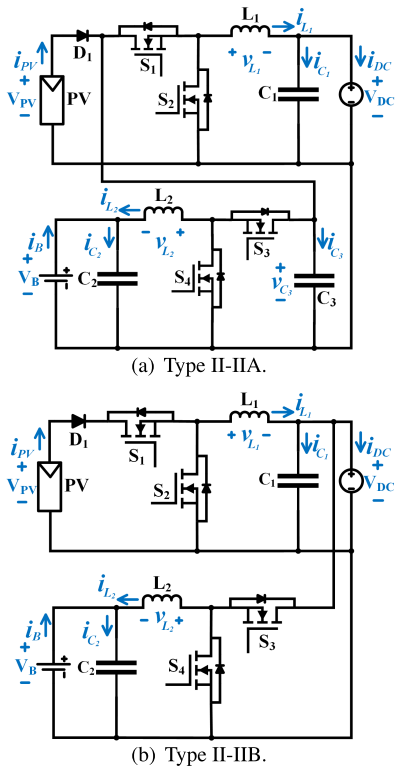
(a) Type II-IIA.

(b) Type II-IIB.

FIGURE 1. The TPC circuits.

The converter is working as a double-input single-output (DISO) converter.

5) **PV and DC bus to battery:** This mode is activated when the battery is low in SoC but the PV source alone is not sufficient to charge the battery at the rated current. Therefore, The converter is working as a DISO converter.

6) **Battery to DC bus:** This mode is activated when the PV source is unable to supply power to the DC bus during night time or under heavily shaded condition.

7) **DC bus to Battery:** This mode is activated when the PV is unable to supply power to the load during night time or under heavily shaded condition. In addition, the battery is low in SoC and would require charging from the DC Bus.

B. TYPE II-IIA STEADY-STATE ANALYSIS

Here, S_1 and S_2 are working as one pair and S_3 and S_4 as another pair. The duty ratio between S_1 and S_3 is depending on the voltage ratio between the DC bus and the battery. When S_1 is turned ON while S_2 is OFF, L_1 starts to charge from the PV source and when S_1 is turned OFF, L_1 starts to discharge. Similarly, when S_3 is turned ON while S_4 is OFF, L_2 starts to charge and vice versa.

1) **PV to DC bus:** The TPC is working as a single-input single-output (SISO) operation between the PV source and the DC bus where the battery is idle in this case. S_1 and S_2 are working in a complementary manner
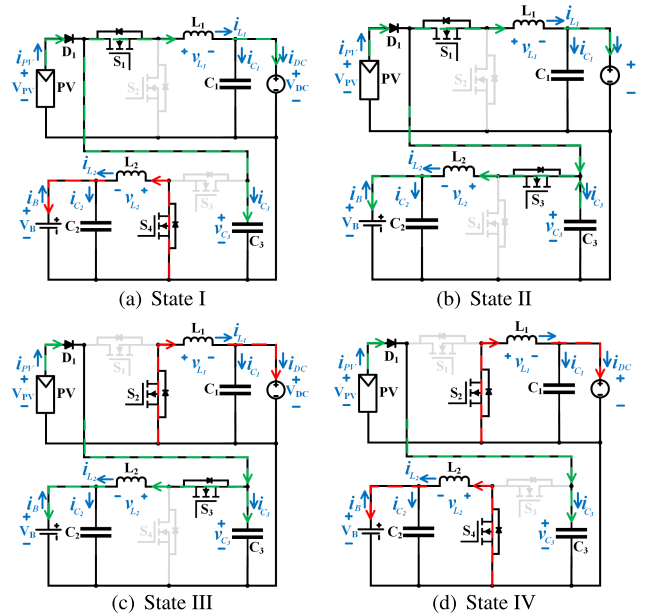

(a) State I   (b) State II

(c) State III   (d) State IV

FIGURE 2. Mode 3 SIDO of Type II-IIA.

while S_3 and S_4 are OFF. This operating mode has two switching states.

2) **PV to battery:** The TPC is working as a SISO converter where the DC bus is idle. S_3 and S_4 are receiving PWM signal and working in a complementary manner while S_1 and S_2 are OFF. This operating mode has two switching states.

3) **PV to DC bus and battery:** The system now operates as a SIDO converter. The duty ratio between S_1 and S_3 is depending on the voltage ratio between the DC bus and the battery given in (1). This operating mode has four switching states as shown in Fig. 2.

$$\frac{V_{DC}}{V_B} = \frac{D_1}{D_3} \tag{1}$$

4) **PV and battery to DC bus**: The TPC is working as a DISO converter. All switches are working in this mode. However, the duty ratio will be higher than Mode 3. This operating mode has four switching states as shown in Fig. 3.

5) **PV and DC bus to battery**: The TPC is working as a DISO converter. All switches are active. However, the duty ratio will be lower than in Mode 3. This operating mode has four switching states as shown in Fig. 4.

6) **Battery to DC bus**: The TPC is working as a SISO converter between the battery and the DC bus. S_3 and S_4 are working as a pair and S_1 and S_2 are ON and OFF respectively to maintain a single conversion stage. This operating mode has two switching states.

7) **DC bus to battery**: The TPC is working as a SISO converter and will be the same as Mode 6. This operating mode has two switching states.

H. Aljarajreh *et al.*: Method of Seamless Transitions Between Different Operating Modes for Three-Port DC-DC Converters

IEEE *Access*

TABLE 1. Switching look-up table for different modes of converter in Fig. 1(a).

Modes	Power	Active Components	State	Switch state ON	Switch state OFF	Duty condition	Fig
PV to DC bus	$P_{pv} = P_{DC}$	D_1, S_1, S_2, L_1, C_1 & C_3	I	S_1^*	S_2^*	—	—
			II	S_2^*	S_1^*	—	—
PV to battery	$P_{pv} = P_B$	D_1, S_3, S_4, L_2, C_2 & C_3	I	S_3^*	S_4^*	—	—
			II	S_4^*	S_3^*	—	—
PV to DC bus and battery	$P_{pv} = P_{DC} + P_B$	All active	I	S_1^*, S_4^*	S_2^*, S_3^*	$\dfrac{D_1}{D_3} \approx \dfrac{V_{DC}}{V_B}$	Fig. 2(a)
			II	S_1^*, S_3^*	S_2^*, S_4^*		Fig. 2(b)
			III	S_2^*, S_3^*	S_1^*, S_4^*		Fig. 2(c)
			IV	S_2^*, S_4^*	S_1^*, S_3^*		Fig. 2(d)
PV and battery to DC bus	$P_{pv} + P_B = P_{DC}$	All active	I	S_1^*, S_4^*	S_2^*, S_3^*	$\dfrac{D_1}{D_3} \geqslant \dfrac{V_{DC}}{V_B}$	Fig. 3(a)
			II	S_1^*, S_3^*	S_2^*, S_4^*		Fig. 3(b)
			III	S_2^*, S_3^*	S_1^*, S_4^*		Fig. 3(c)
			IV	S_2^*, S_4^*	S_1^*, S_3^*		Fig. 3(d)
PV and DC bus to battery	$P_{pv} + P_{DC} = P_B$	All active	I	S_1^*, S_4^*	S_2^*, S_3^*	$\dfrac{D_1}{D_3} \leqslant \dfrac{V_{DC}}{V_B}$	Fig. 4(a)
			II	S_1^*, S_3^*	S_2^*, S_4^*		Fig. 4(b)
			III	S_2^*, S_3^*	S_1^*, S_4^*		Fig. 4(c)
			IV	S_2^*, S_4^*	S_1^*, S_3^*		Fig. 4(d)
battery to DC bus	$P_B = P_{DC}$	All active except D_1, S_2	I	S_1°, S_4^*	S_3^*	—	—
			II	S_1°, S_3^*	S_4^*	—	—
DC bus to battery	$P_{DC} = P_B$	All active except D_1, S_2	I	S_1°, S_4^*	S_3^*	—	—
			II	S_1°, S_3^*	S_4^*	—	—

* Switch operates in PWM   ° Switch is fully ON

(a) State I   (b) State II

(c) State III   (d) State IV

FIGURE 3. Mode 4 DISO of Type II-IIA.

(a) State I   (b) State II

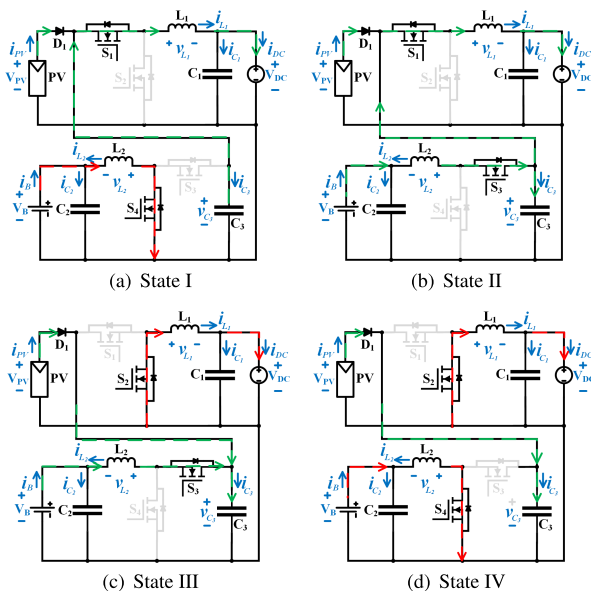(c) State III   (d) State IV

FIGURE 4. Mode 5 DISO of Type II-IIA.

The switching patterns to achieve all seven modes of operation are shown in Table 1. Although there are four switches in the converter, only two sets of PWM are required to implement all modes.

C. TYPE II-IIB STEADY-STATE ANALYSIS

1) **PV to DC bus:** S_1 and S_2 are working in a complementary manner while S_3 and S_4 are OFF. This operating mode has two switching states.

2) **PV to battery:** S_1 and S_2 are receiving the PWM signal and working in a complementary manner while S_3 is ON and S_4 is OFF to maintain a single conversion stage. This operating mode has two switching states.
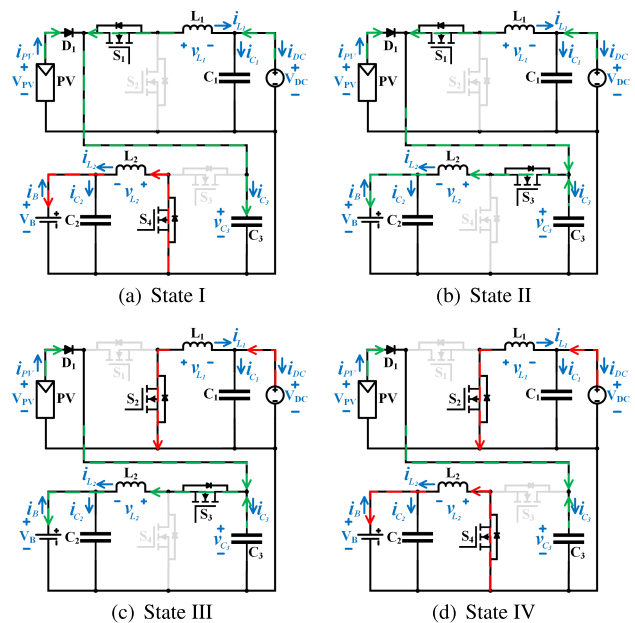
3) **PV to DC bus and battery**: The system now operates as a SIDO converter. The ratio between the DC bus and the battery is given in (2). This operating mode has four switching states as shown in Fig. 5.

$$\frac{V_{DC}}{V_B} = \frac{1}{D_3} \qquad (2)$$

4) **PV and battery to DC bus**: The TPC is working as a DISO converter. All switches are active. However, the duty ratio of these PWM signals are different from those in Mode 3. This operating mode has four switching states as shown in Fig. 6.
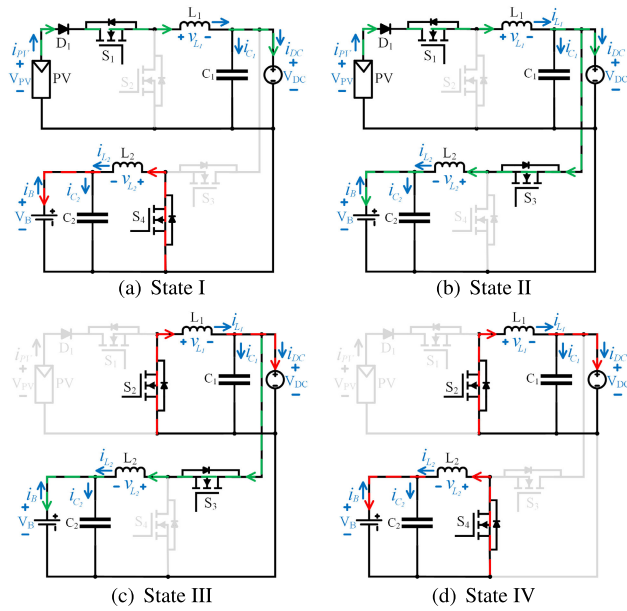
IEEE Access

H. Aljarajreh *et al.*: Method of Seamless Transitions Between Different Operating Modes for Three-Port DC-DC Converters
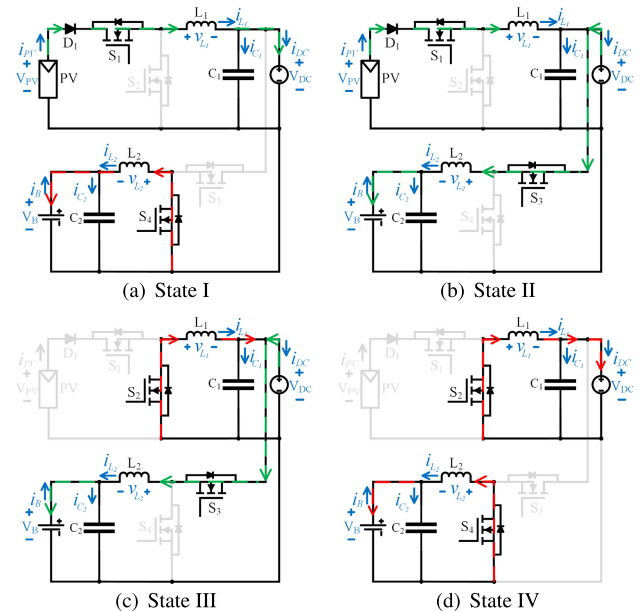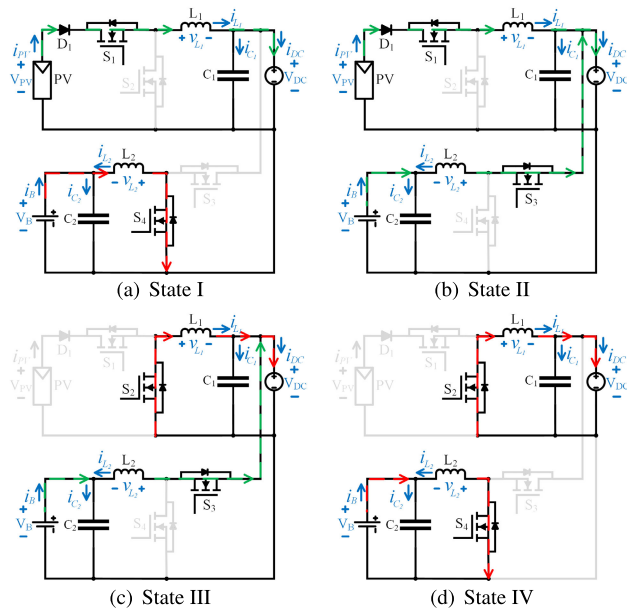

FIGURE 5. Mode 3 SIDO of Type II-IIB.

FIGURE 6. Mode 4 DISO of Type II-IIB.

5) **PV and DC bus to battery**: The TPC is working as a DISO converter. All switches are active. This operating mode has four switching states, as shown in Fig. 7.

6) **battery to DC bus**: The TPC is working between the battery and the DC bus as a SISO converter. This operating mode has two switching states.

7) **DC bus to battery**: S_3 and S_4 are receiving the PWM signals and working in a complementary manner while S_1 and S_2 are OFF. This operating mode has two switching states.

The switching patterns to achieve all seven modes of operation are shown in Table 2.

FIGURE 7. Mode 5 DISO of Type II-IIB.

D. INDUCTORS AND CAPACITORS DESIGN

As the converter is designed to work in continuous conduction mode the minimum inductor and capacitor equations are given below:

$$L_1 = \frac{(V_{PV} - V_{DC})}{\Delta i_{L_1} f} D_1 \tag{3}$$

$$C_1 = \frac{(1 - D_1)V_{DC}}{8L_1 f^2 \Delta V_{DC}} \tag{4}$$

$$L_2 = \frac{(V_{PV} - V_B)}{\Delta i_{L_2} f} D_3 \tag{5}$$

$$C_2 = \frac{(1 - D_3)V_B}{8L_2 f^2 \Delta V_B} \tag{6}$$

The worst case, which is DISO in Mode 5, is used to calculate C_3,

$$C_3 = \frac{[i_{L_1}(t_d) - i_{L_1(max)}]t_d + [(1 - D_3)T - t_d]I_{PV}}{\Delta V_{PV}} \tag{7}$$

III. CONTROL STRUCTURE AND MODE SELECTION

The three-port converter topology consists of two pairs of switches where in each pair the switches are working complementary during different modes. Both switches of these complementary pairs will turn on/off according to the requirements of the modes. The control arrangement loops, namely MPPT, battery protection and output voltage regulation. MPPT is achieved through the first pair S_1 & S_2, while S_3 & S_4 are responsible for both output voltage regulation (PI controller) and battery protection. Texas Instrument DSP controller (TMS320F28379D) is used to control the converter. The three-port converter is constructed based on basic buck and boost converters. The transfer functions of buck and boost converters are given in many literatures as in [33]. To make

H. Aljarajreh *et al.*: Method of Seamless Transitions Between Different Operating Modes for Three-Port DC-DC Converters

IEEE Access

TABLE 2. Switching look-up table for different modes of converter in Fig. 1(b).

Modes	Power	Active Components	State	Switch state ON	Switch state OFF	Duty condition	Fig
PV to DC bus	$P_{pv} = P_{DC}$	$D_1, S_1, S_2, L_1 \& C_1$	I	S_1^*	S_2^*	–	–
			II	S_2^*	S_1^*	–	–
PV to battery	$P_{pv} = P_B$	All active except S_4	I	S_1^*, S_3°	S_2^*	–	–
			II	S_2^*, S_3°	S_1^*	–	–
PV to DC bus and battery	$P_{pv} = P_{DC} + P_B$	All active	I	S_1^*, S_4^*	S_2^*, S_3^*	$\frac{1}{D_3} \approx \frac{V_{DC}}{V_B}$	Fig. 5(a)
			II	S_1^*, S_3^*	S_2^*, S_4^*		Fig. 5(b)
			III	S_2^*, S_3^*	S_1^*, S_4^*		Fig. 5(c)
			IV	S_2^*, S_4^*	S_1^*, S_3^*		Fig. 5(d)
PV and battery to DC bus	$P_{pv} + P_B = P_{DC}$	All active	I	S_1^*, S_4^*	S_2^*, S_3^*	$\frac{1}{D_3} \geqslant \frac{V_{DC}}{V_B}$	Fig. 6(a)
			II	S_1^*, S_3^*	S_2^*, S_4^*		Fig. 6(b)
			III	S_2^*, S_3^*	S_1^*, S_4^*		Fig. 6(c)
			IV	S_2^*, S_4^*	S_1^*, S_3^*		Fig. 6(d)
PV and DC bus to battery	$P_{pv} + P_{DC} = P_B$	All active	I	S_1^*, S_4^*	S_2^*, S_3^*	$\frac{1}{D_3} \leqslant \frac{V_{DC}}{V_B}$	Fig. 7(a)
			II	S_1^*, S_3^*	S_2^*, S_4^*		Fig. 7(b)
			III	S_2^*, S_3^*	S_1^*, S_4^*		Fig. 7(c)
			IV	S_2^*, S_4^*	S_1^*, S_3^*		Fig. 7(d)
battery to DC bus	$P_B = P_{DC}$	$S_3, S_4, L_2, C_1 \& C_2$	I	S_3^*	S_4^*	–	–
			II	S_4^*	S_3^*	–	–
DC bus to battery	$P_{DC} = P_B$	$S_3, S_4, L_2, C_1 \& C_2$	I	S_3^*	S_4^*	–	–
			II	S_4^*	S_3^*	–	–

* Switch operates in PWM   ° Switch is fully ON

the buck converter model more precise, many parameters have been added to the basic transfer function as in [34]. After substituting all components values in the transfer function as in (8) & (9), Matlab is used to find the Z-transform of the transfer function using zero-order hold (ZOH) model as in (10). Then, the margin stability bode plot and root locus tools are used to find the controller transfer function as in (11) and the step response of the closed-loop system where $K_a = k_p$ and $K_b = k_i T_s - k_p$ as shown in Fig. 8. For the buck converter, $K_a = 0.2$ and $K_b = -0.19$ which used in DSP to control the converter.

$$G_{vd}(s) = \frac{\frac{RV_i}{LC(R+r_c)}(r_c Cs + 1)}{s^2 + (\frac{1}{L}(r_L + r_c) + \frac{1}{C(R+r_c)})s + \frac{r_L + R}{LC(R+r_c)}} \quad (8)$$

$$G_{vd}(s) = \frac{0.04446s + 370.5}{5.346e^{-7}s^2 + 0.002146s + 15.01} \quad (9)$$

$$G_{vd}(z) = \frac{1.73z - 1.464}{z^2 - 1.912z + 0.9228} \quad (10)$$

$$G_c(z) = \frac{0.2z - 0.19}{z - 1} \quad (11)$$

Similarly, the transfer function of boost converter is obtained as in (12) and the controller function in (13). The step response of the closed-loop system of boost converter is presented in Fig. 9 and the parameters are $K_a = 0.0004$ and $K_b = -0.00032$.

$$G_{vd}(z) = \frac{-3.36z^2 + 6.794z - 3.176}{z^2 - 1.975z + 0.9802} \quad (12)$$

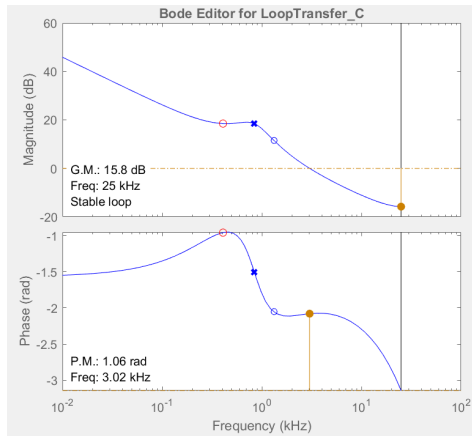$$G_c(z) = \frac{0.0004z - 0.00032}{z - 1} \quad (13)$$

The working of the two pairs of complementary switches can be conveniently explained with the help of Table 1 and

Table 2. There are four SISO modes (1, 2, 6 & 7) in which only one pair of switches is receiving PWM signals. However, it is worth mentioning that in Modes 6 & 7, S_1 is always on while S_2 is always off to achieve single-stage power conversion. In the remaining modes, all switches receive PWM signals. Based on the available power and load power demand, the mode is selected automatically. It is evident that there are 7 different modes toggling from one mode to another according to the conditions.
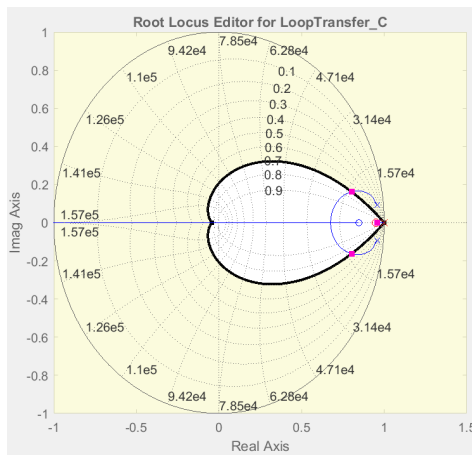
The aforementioned switching requirements in different modes present a challenge in designing a proper switching strategy that optimizes the conversion efficiency, manages system delays and fulfills the control objectives. To show the merits and feasibility of the proposed method, different scenarios are considered for comparison with conventional practice:

Case 1: The "no PV power" scenario is activated when the PV power is set to 0 W. In practice, the PV power is larger than 0 W during daylight even in cloudy or stormy weather condition and thus the power threshold should be defined. Conventionally, the converter turns OFF to avoid losses. However, if the generated power from the PV source is higher than the losses, it is worth keeping the converter ON, as in the proposed method and using this power instead of losing it all. This will also simplify the control patterns, making the one pattern control possible. For example, 1% of 30 W power is 0.3 W and the condition is to turn the converter ON if the PV power is higher than 0.3 W, even when the loss in the converter is 0.1 W.
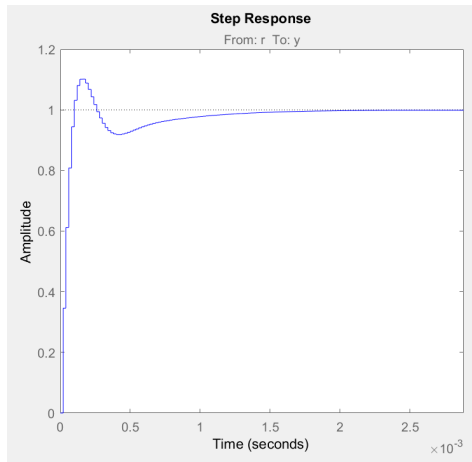
Case 2: If the converter that is connected to the PV source is turned OFF, the PV power may not be able to measure unless additional light sensor is used which increase the cost and the complexity. Another way is to deliberately turn ON the converter periodically (such as in every 2 s) to check the

IEEE *Access*

H. Aljarajreh *et al.*: Method of Seamless Transitions Between Different Operating Modes for Three-Port DC-DC Converters

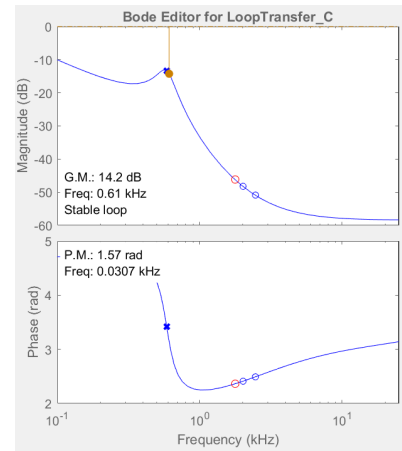

(a) Margin stability bode plot

(b) Root locus of the closed loop transfer function

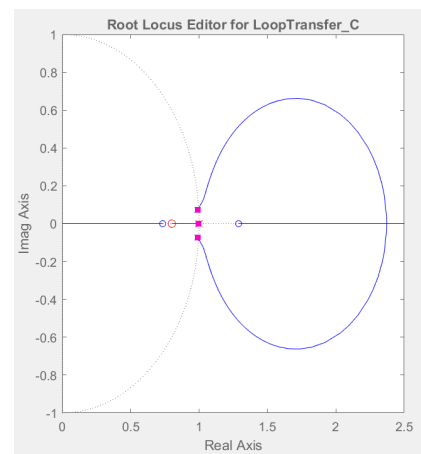
(c) Step response

FIGURE 8. Bode plot, Root locus of the closed-loop transfer function and the step response of the buck converter.

(a) Margin stability bode plot

(b) Root locus of the closed loop transfer function

(c) Step response

FIGURE 9. Bode plot, Root locus of the closed-loop transfer function and the step response of the boost converter.
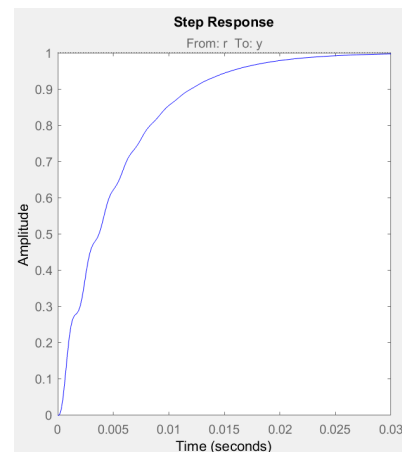
PV power availability. In the proposed method, the converter is always ON and it would not run into this situation except when the PV power is close to 0 W for a long time such as during night time. Once the converter becomes OFF the V_{OC} is used as an indicator to turn ON the converter and measure the power if it is more than the threshold, as shown in the left side of Fig. 12.

Case 3: Conventionally in PV to DC bus mode, the converter that is connected to the battery is turned OFF, and in this case there is no output voltage regulation, where one control objective will be sacrificed. In addition, it is rarely to have PV power exactly equal output power but a constant variation above or below the output load power. In the proposed
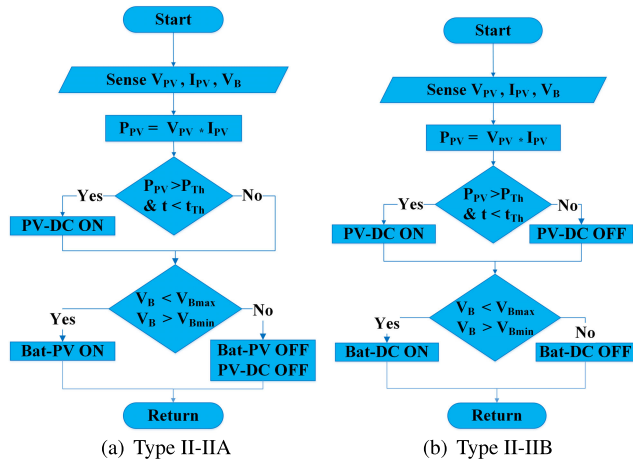
H. Aljarajreh *et al.*: Method of Seamless Transitions Between Different Operating Modes for Three-Port DC-DC Converters

IEEE *Access*

(a) Type II-IIA   (b) Type II-IIB

FIGURE 10. Flowchart of the proposed method with only 2 conditions to implement all 7 modes of operation for both converter.

method, when PV power is close to the power of DC bus there is no need to check $P_{PV} = P_{DC}$ condition and turns the converter OFF as in the conventional method because there is no power injecting from the battery.

Case 4: Every mode transition takes 2 s to be active. The reason is to ensure steady measurements. For example, if the battery voltage exceeds the maximum voltage, the second pair (S_3 & S_4) turns OFF to protect the battery. As a result after short period of time the battery voltage reaches slightly lower than the maximum voltage and turns ON. If the update is very fast, the system turns the converter ON and OFF at similar speed. As a result the switching losses would increase in proportion to the frequency at which it switches. In Fig. 12(b), the minimum response time of the commercial PV emulator used in this experiment is 1 s. Therefore, minimum 2 s update is needed to ensure steady measurements. However, the proposed method reduces the selection conditions and simplifies the decision making process with less frequent updates.

A. THE PROPOSED METHOD

In order to get rid of the complex switching patterns and the associated control design, a new criterion for mode selection has been proposed where both pairs of the switches are receiving PWM signals all the time. The power loss when there is no input power is found by LTspice to be around 0.1 W for the proposed method which means less than 1% degradation of the efficiency. The first pair (S_1 & S_2) will be responsible for MPPT while the second pair (S_3 & S_4) is regulating the output voltage. In battery to DC bus mode, no power is being transferred by S_1 & S_2 as there is no PV power. On the other hand, S_3 & S_4 are transferring power from battery to DC bus. Furthermore, the PV to DC bus mode can be achieved when the PV power is equal to the power of DC bus. This power will not be coming from the battery even it is connected. In PV to battery mode, the power will be transferred from PV to battery under no-load condition. In this way, the converter is moving from one mode to another irrespective of any conditions. This makes a single pattern

TABLE 3. Component specification.

Parameter	Value
Controller	TMS320f28379D
Battery	12 V, 7.2 A
PV emulator	ELEKTRO-AUTOMATIK EA-PSI 9360-15 (30 W)
Output	ELEKTRO-AUTOMATIK EA-EL 9750-25
MOSFETs	IRF540Z
D_1	STPS10L25D
L_1 and L_2	330 uH
C_1 and C_2	100 uF
f_s	50 KHz
C_3	120 uF

control for all the three ports of the converter possible. In the conventional way, 3 current sensors, 3 voltage sensors and 1 irradiation sensor are needed for the proposed method. However, only 1 current sensor and 3 voltage sensors are used. In this method there are only two conditions namely, the battery being over-charged or discharged and the PV power being under the threshold for a long time such as during night time, as shown in Fig. 10. In this work, the output is a resistive load where a linear controller can satisfy the stability of the system. However, if the output is a constant power load (CPL) there is no guarantee that the control performance will be satisfactory for all operating range. However, this problem has been well rehearsed in literature [35], where an observer-based dc voltage droop and current feed-forward control is presented. In addition, authors in [36] proposed a novel Composite Nonlinear Controller for Stabilization of Constant Power Load. Furthermore, feedforward terms are added to V-I droop-based dual-loop controller to ensure the exponential stability in the whole operating range [37]. These methods are applicable to TPCs which will be our future work as it requires extensive analysis and it is not the scope of this paper. Nevertheless, the main contribution is designing three-port converters (TPCs) for smooth transitions with 7 distinctive operating modes.

IV. EXPERIMENTAL RESULTS

The experimental setup of Type II-IIA and Type II-IIB circuits is shown in Fig. 11(a). A hardware prototype is built as in Fig. 11(b) and tested based on Fig. 1(a), and then modified based on Fig. 1(b). The components used in the circuit are listed in Table 3. Simple voltage divider is used to sense the voltage of each port as shown in Fig. 11(b). In addition, ACS712 current sensor is connected to the PV port. The experimental waveforms and transient responses of changing from one mode to another for Type II-IIA and Type II-IIB converters are shown in Figs. 13 and 14, respectively.

In Fig. 13, the order of these four traces from top view to bottom view are PV voltage, output voltage, first inductor current and battery current respectively. A PV emulator is used and a simple Perturb and Observe (P&O) is used to achieve MPPT where $V_{MPP} = 23$ V. The output port is connected to an electronic load which is programmed as Constant Voltage (CV) at 15 V. In Fig. 13(a), battery current is zero

IEEE *Access*

H. Aljarajreh *et al.*: Method of Seamless Transitions Between Different Operating Modes for Three-Port DC-DC Converters

TABLE 4. Comparison between the proposed method and others.

| Reference	Modes	Delay	Overshoot	Settling time	Complex control	Selection Conditions	Modes Transition	Sensors
[15]	3	-	-	-	Mid	3	Simulation results	6
[16]	3	-	-	-	-	Not shown	Simulation results	5
[17]	3	-	-	-	Mid	3	Simulation results	Not considered
[18]	3	-	-	-	Mid	3	Simulation results	6
[19]	4	-	-	-	Mid	4	Not considered	5
[20]	4	-	-	-	Mid	3	One case only	5
[21]	4	-	-	-	-	3	Not considered	4
[22]	4	-	-	-	Mid	3	Not considered	6
[23]	5	No	10%	0.4 s	High	5	Experimental	6
[24]	4	No	40%	0.2 s	Mid	4	Experimental	6
[25]	7	Yes	20%	1 s	High	4	Experimental	5
[26]	7	Yes	No	1 s	High	4	Experimental	5
[30]	4	No	50%	0.6 s	Mid	4	Experimental	6
[31]	6	-	-	-	Mid	3	Simulation results	5
[32]	6	Yes	-	-	Mid	4	Experimental	6
[38]	3	No	10%	0.2 s	Mid	3	Experimental	6
[39]	3	No	10%	0.2 s	Low	2	Experimental	6
[40]	3	No	30%	0.3 s	Mid	3	Experimental	6
Proposed	7	No	10%	0.1 s	Low	2	Experimental	4
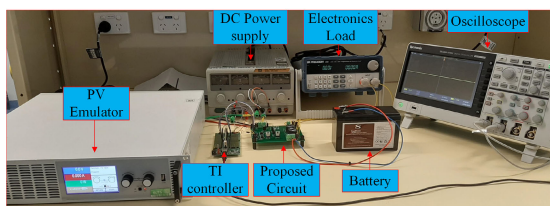
(a) Experimental setup of the proposed circuit
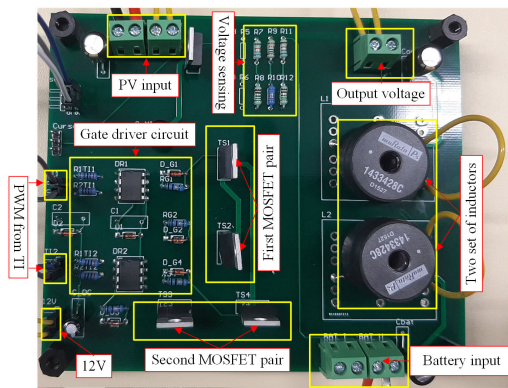

(b) Hardware prototype of Type II-IIA circuit

FIGURE 11. Experimental setup and the prototype of the circuit.
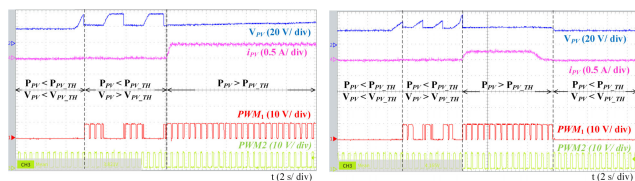
(a) Buck converter operates with the PV power and V_{OC} as indicators with 2 s update.

(b) Buck converter operates with the PV power and V_{OC} as indicators with 1 s update.
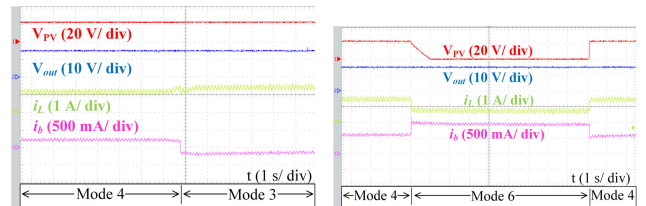
FIGURE 12. The power conditions of the upper converter (buck) of Type II-IIB.

as the PV source supplies power to the DC bus only and the inductor current is approximately 2 A. Then, in Fig. 13(b), DC bus is not connected (i.e., $V_{DC} = 0$). The current from the battery is negative to indicate that the battery is charging.
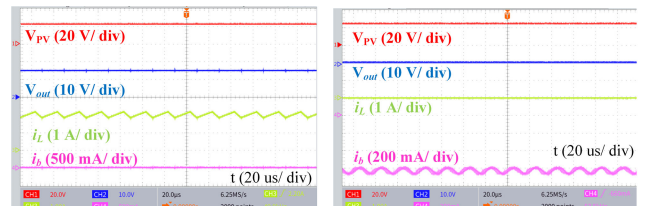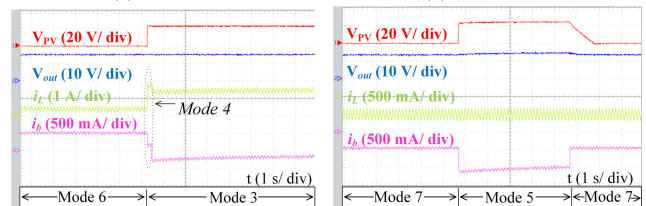

(a) Mode 1 (PV to DC bus)

(b) Mode 2 (PV to battery)

(c) Mode 3-4

(d) Mode 4-6-4

(e) Mode 6-4-3

(f) Mode 7-5-7

FIGURE 13. Waveforms of Type II-IIA converter.

Fig. 13(c) shows the transient response of transition from Mode 4 (where PV and battery are supplying power to the DC bus and when PV is able to supply both DC bus and battery) switched to Mode 3 (where the battery current changed the direction to charging). Fig. 13(d) shows the transient response of transition from Mode 4 to Mode 6 or vice-versa, the PV source and battery are supplying power to the DC bus and when PV does not have enough power, the battery can power the DC bus and increase the battery's current to cover absence of the PV source. Fig. 13(e) shows the transient response of transition from Mode 6 to Mode 3, the battery is discharging to the DC bus. When PV has power to supply the battery and
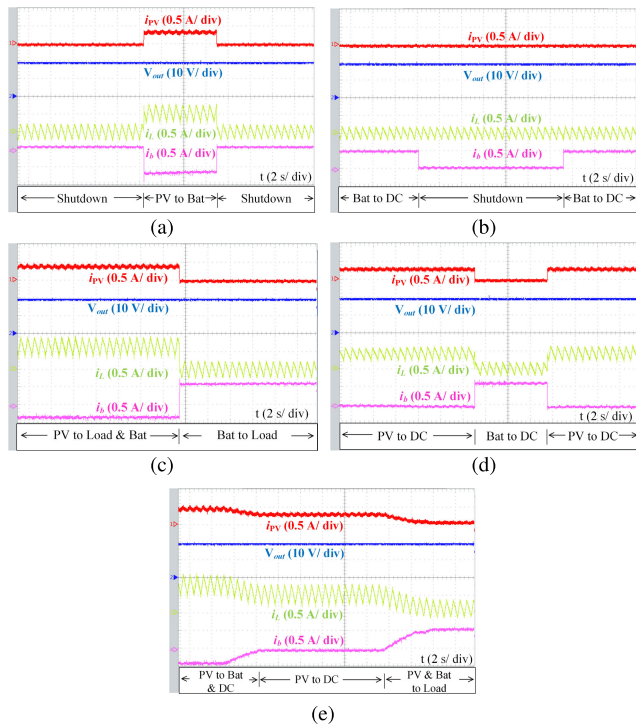
H. Aljarajreh *et al.*: Method of Seamless Transitions Between Different Operating Modes for Three-Port DC-DC Converters

IEEE *Access*

FIGURE 14. Waveforms of Type II-IIB converter.

DC bus at the same time, the system will pass through Mode 4 for a small period of time, typically less than half a second, and then will reach Mode 6 in the steady state. Fig. 13(f) shows the transient response from Mode 5 to Mode 7. The DC bus is supplying the battery then PV has some power with DC bus to supply the battery. Therefore, the battery's current continues to charge but at a higher level when the PV source has excess power.

The transition response of Type II-IIB converter is shown in Fig. 14. Fig. 14(a) shows a step response from PV emulator with no load. Fig. 14(b) shows a step response in the load at no PV power. Fig. 14(c) shows a step change in PV power to 0 and battery supplies the load. Fig. 14(d) shows PV power only supplies load and then battery supplies the load. Finally, Fig. 14(e) shows continuous change in PV power to show the controllability of the converters in different modes.

V. CONCLUSION

Conventionally, mode transition is achieved by assigning specific switching patterns through feedback signals and control algorithms. Defining a power threshold, ensuring smooth transition, achieving fast response, minimizing sensor error and time to update are issues in the conventional mode selection. A mechanism for ensuring fast and smooth transitions of operating modes for three-port converters is presented in this paper. In addition, this work considers two bidirectional ports as compared to only one bidirectional port in most reported topologies. This configuration enables both standalone and grid-connected applications. MPPT, battery protection and output voltage regulation are achieved. In the proposed method, the number of switching patterns is significantly

reduced and decisions are simplified for all modes. The transitions between modes are achieved with fast settling time and no obvious overshoot and undershoot. Based on the power availability and load demand, the mode is activated automatically. The proposed control strategy and mechanism for TPC have potential applications in the DC microgrid.

REFERENCES

[1] N. D. Dao, D.-C. Lee, and Q. D. Phan, "High-efficiency SiC-based isolated three-port DC/DC converters for hybrid charging stations," *IEEE Trans. Power Electron.*, vol. 35, no. 10, pp. 10455–10465, Oct. 2020.

[2] G. R. C. Mouli, J. Schijffelen, M. van den Heuvel, M. Kardolus, and P. Bauer, "A 10 kW solar-powered bidirectional EV charger compatible with chademo and COMBO," *IEEE Trans. Power Electron.*, vol. 34, no. 2, pp. 1082–1098, Feb. 2019.

[3] D.-D. Nguyen, G. Fujita, and M. C. Ta, "A new soft-switching strategy for three-port converter to be applied in EV application," in *Proc. IEEE 3rd Int. Future Energy Electron. Conf. ECCE Asia (IFEEC-ECCE Asia)*, Jun. 2017, pp. 1126–1131.

[4] S.-K. Kim, J.-H. Jeon, C.-H. Cho, J.-B. Ahn, and S.-H. Kwon, "Dynamic modeling and control of a grid-connected hybrid generation system with versatile power transfer," *IEEE Trans. Ind. Electron.*, vol. 55, no. 4, pp. 1677–1688, Apr. 2008.

[5] K. Jin, X. Ruan, M. Yang, and M. Xu, "A hybrid fuel cell power system," *IEEE Trans. Power Electron.*, vol. 56, no. 4, pp. 1212–1222, Apr. 2009.

[6] A. Ganjavi, H. Ghoreishy, A. A. Ahmad, and Z. Zhagn, "A three-level three-port bidirectional DC–DC converter," in *Proc. IEEE Int. Power Electron. Appl. Conf. Exposit. (PEAC)*, Nov. 2018, pp. 1–4.

[7] S. Gao, J. Shi, X. Dong, Y. Jia, H. Wu, and H. Hu, "Performance evaluation of a non-isolated three-port converter for PV-battery hybrid energy system," in *Proc. 44th Annu. Conf. IEEE Ind. Electron. Soc. (IECON)*, Oct. 2018, pp. 1394–1399.

[8] S. Wen, S. Wang, G. Liu, and R. Liu, "Energy management and coordinated control strategy of PV/HESS AC microgrid during islanded operation," *IEEE Access*, vol. 7, pp. 4432–4441, 2019.

[9] P. Yang, C. K. Tse, J. Xu, and G. Zhou, "Synthesis and analysis of double-input single-output DC/DC converters," *IEEE Trans. Ind. Electron.*, vol. 62, no. 10, pp. 6284–6295, Oct. 2015.

[10] Z. Wang, Q. Luo, Y. Wei, D. Mou, X. Lu, and P. Sun, "Topology analysis and review of three-port DC–DC converters," *IEEE Trans. Power Electron.*, vol. 35, no. 11, pp. 11783–11800, Nov. 2020.

[11] C. G. Zogogianni, E. C. Tatakis, and M. S. Vekic, "Non-isolated reduced redundant power processing DC/DC converters: A systematic study of topologies with wide voltage ratio for high-power applications," *IEEE Trans. Power Electron.*, vol. 34, no. 9, pp. 8491–8502, Sep. 2019.

[12] M. Waseem, L. Saeed, M. Y. A. Khan, J. Saleem, and A. Majid, "A multi input multi output bidirectional DC–DC boost converter with backup battery port," in *Proc. 1st Int. Conf. Power, Energy Smart Grid (ICPESG)*, Apr. 2018, pp. 1–6.

[13] H. Moradisizkoohi, N. Elsayad, and O. A. Mohammed, "A family of three-port three-level converter based on asymmetrical bidirectional half-bridge topology for fuel cell electric vehicle applications," *IEEE Trans. Power Electron.*, vol. 34, no. 12, pp. 11706–11724, Dec. 2019.

[14] H. Aljarajreh, D. D.-C. Lu, and C. K. Tse, "Synthesis of dual-input single-output DC/DC converters," in *Proc. IEEE Int. Symp. Circuits Syst. (ISCAS)*, May 2019, pp. 1–5.

[15] H. Khoramikia, M. Heydari, and S. M. Dehghan, "A new three-port non-isolated DC–DC converter for renewable energy sources application," in *Proc. Electr. Eng. (ICEE), Iranian Conf.*, May 2018, pp. 1101–1106.

[16] S. Bhattacharya and S. Samanta, "A novel non-isolated three port DC–DC converter for photovoltaic applications," in *Proc. IEEE Int. Conf. Power Electron., Smart Grid Renew. Energy (PESGRE)*, Jan. 2020, pp. 1–6.

[17] X. Qi, D. Zhang, X. Pan, and M. Fang, "A coupled inductors based high gain non-isolated three-port DC–DC converter," in *Proc. IEEE Int. Power Electron. Appl. Conf. Exposit. (PEAC)*, Nov. 2018, pp. 1–6.

[18] N. Zahedi, S. Salehi, and S. H. Hosseini, "Non-isolated three port DC–DC converter with soft switching technique," in *Proc. 10th Int. Power Electron., Drive Syst. Technol. Conf. (PEDSTC)*, Feb. 2019, pp. 401–406.

IEEE Access

H. Aljarajreh *et al.*: Method of Seamless Transitions Between Different Operating Modes for Three-Port DC-DC Converters

[19] R. Faraji, H. Farzanehfard, M. Esteki, and S. A. Khajehoddin, "A lossless passive snubber circuit for three-port DC–DC converter," *IEEE J. Emerg. Sel. Topics Power Electron.*, vol. 9, no. 2, pp. 1905–1914, Aug. 2021.

[20] R. Cheraghi, E. Adib, and M. S. Golsorkhi, "A non-isolated high step-up three-port soft-switched converter with minimum switches," *IEEE Trans. Ind. Electron.*, early access, Sep. 29, 2020, doi: 10.1109/TIE.2020.3026306.

[21] B. Honarjoo, S. M. Madani, M. Niroomand, and E. Adib, "Non-isolated high step-up three-port converter with single magnetic element for photovoltaic systems," *IET Power Electron.*, vol. 11, no. 13, pp. 2151–2160, Nov. 2018.

[22] M. Al-Soeidat, H. Khawaldeh, D. D.-C. Lu, and J. Zhu, "A novel high step-up three-port bidirectional DC/DC converter for PV-battery integrated system," in *Proc. IEEE Appl. Power Electron. Conf. Exposit. (APEC)*, Mar. 2020, pp. 3352–3357.

[23] M. R. Al-Soeidat, H. Aljarajreh, H. A. Khawaldeh, D. D. C. Lu, and J. Zhu, "A reconfigurable three-port DC–DC converter for integrated PV-battery system," *IEEE J. Emerg. Sel. Topics Power Electron.*, vol. 8, no. 4, pp. 3423–3433, Dec. 2020.

[24] B. Zhang, P. Wang, T. Bei, X. Li, Y. Che, and G. Wang, "Novel topology and control of a non-isolated three port DC–DC converter for PV-battery power system," in *Proc. 20th Int. Conf. Electr. Mach. Syst. (ICEMS)*, Aug. 2017, pp. 1–6.

[25] T. Cheng and D. D.-C. Lu, "Three-port converters with a flexible power flow for integrating PV and energy storage into a DC bus," *J. Power Electron.*, vol. 17, no. 6, pp. 1433–1444, Jun. 2017.

[26] T. Cheng, D. D.-C. Lu, and L. Qin, "Non-isolated single-inductor DC/DC converter with fully reconfigurable structure for renewable energy applications," *IEEE Trans. Circuits Syst. II, Exp. Briefs*, vol. 65, no. 3, pp. 351–355, Mar. 2018.

[27] Q. Wang, D. Zha, M. Cheng, F. Deng, and G. Buja, "Energy management system for DC electric spring with parallel topology," *IEEE Trans. Ind. Appl.*, vol. 56, no. 5, pp. 5385–5395, Sep. 2020.

[28] I. Askarian, M. Pahlevani, and A. M. Knight, "Three-port bidirectional DC/DC converter for DC nanogrids," *IEEE Trans. Power Electron.*, vol. 36, no. 7, pp. 8000–8011, Jul. 2021.

[29] Y.-E. Wu and I.-C. Chen, "Novel integrated three-port bidirectional DC/DC converter for energy storage system," *IEEE Access*, vol. 7, pp. 104601–104612, Jul. 2019.

[30] D. Debnath and K. Chatterjee, "Two-stage solar photovoltaic-based stand-alone scheme having battery as energy storage element for rural deployment," *IEEE Trans. Ind. Electron.*, vol. 62, no. 7, pp. 4148–4157, Jul. 2015.

[31] J. Hong, J. Yin, Y. Liu, J. Peng, and H. Jiang, "Energy management and control strategy of photovoltaic/battery hybrid distributed power generation systems with an integrated three-port power converter," *IEEE Access*, vol. 7, pp. 82838–82847, Jun. 2019.

[32] V. Monteiro, J. G. Pinto, and J. L. Afonso, "Experimental validation of a three-port integrated topology to interface electric vehicles and renewables with the electrical grid," *IEEE Trans. Ind. Informat.*, vol. 14, no. 6, pp. 2364–2374, Jun. 2018.

[33] X.-E. Hong, J.-F. Wu, and C.-L. Wei, "98.1%-efficiency hysteretic-current-mode noninverting buck–boost DC–DC converter with smooth mode transition," *IEEE Trans. Power Electron.*, vol. 32, no. 3, pp. 2008–2017, Mar. 2017.

[34] M. M. Garg, Y. V. Hote, M. K. Pathak, and L. Behera, "An approach for buck converter PI controller design using stability boundary locus," in *Proc. IEEE/PES Transmiss. Distrib. Conf. Exposit. (T&D)*, Apr. 2018, pp. 1–5.

[35] Q. Xu, C. Zhang, C. Wen, and P. Wang, "A novel composite nonlinear controller for stabilization of constant power load in DC microgrid," *IEEE Trans. Smart Grid*, vol. 10, no. 1, pp. 752–761, Jan. 2019.

[36] X. Li, L. Guo, S. Zhang, C. Wang, Y. W. Li, A. Chen, and Y. Feng, "Observer-based DC voltage droop and current feed-forward control of a DC microgrid," *IEEE Trans. Smart Grid*, vol. 9, no. 5, pp. 5207–5216, Sep. 2018.

[37] Y. Gui, R. Han, J. M. Guerrero, J. C. Vasquez, B. Wei, and W. Kim, "Large-signal stability improvement of DC–DC converters in DC microgrid," *IEEE Trans. Energy Convers.*, early access, Feb. 4, 2021, doi: 10.1109/TEC.2021.3057130.

[38] L.-J. Chien, C.-C. Chen, J.-F. Chen, and Y.-P. Hsieh, "Novel three-port converter with high-voltage gain," *IEEE Trans. Power Electron.*, vol. 29, no. 9, pp. 4693–4703, Sep. 2014.

[39] J. Deng, H. Wang, and M. Shang, "A ZVS three-port DC/DC converter for high-voltage bus-based photovoltaic systems," *IEEE Trans. Power Electron.*, vol. 34, no. 11, pp. 10688–10699, Nov. 2019.

[40] H. Wu, K. Sun, S. Ding, and Y. Xing, "Topology derivation of nonisolated three-port DC–DC converters from DIC and DOC," *IEEE Trans. Power Electron.*, vol. 28, no. 7, pp. 3297–3307, Jul. 2013.

HAMZEH ALJARAJREH (Member, IEEE) received the B.Eng. degree in electrical (electronics) engineering from the University of Mu'tah, Alkarak, Jordan, in 2010, and the M.Eng. degree in microelectronics from the Universiti Kebangsaan Malaysia (UKM), Bangi, Malaysia, in 2012. He is currently pursuing the Ph.D. degree with the University of Technology Sydney (UTS), Australia. In 2010, he was a Lab Supervisor with the University of Mu'tah. From 2015 to 2016, he was a Senior Electronic Engineer with Demand Manager Private Ltd. Since 2016, he has been a Casual Academic with UTS for various power electronics subjects. Since 2020, he has also been a Secretary for IEEE NSW IES/IAS/PELS Chapter. His current research interests include designing efficient multiple-input multiple-output DC/DC converters for renewable energy sources, energy storage systems, and microgrids. He is currently a reviewer for several IEEE TRANSACTION journals.
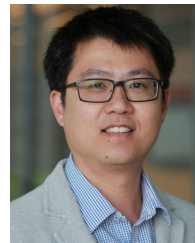
DYLAN DAH-CHUAN LU (Senior Member, IEEE) received the Ph.D. degree in electronic and information engineering from The Hong Kong Polytechnic University, Hong Kong, in 2004. In 2003, he joined Power eLab Ltd., as a Senior Design Engineer, where he was responsible for industrial switching power supply projects. From 2006 to 2016, he was a full-time Faculty Member with The University of Sydney, Australia, where he now holds an honorary position. In July 2016, he joined the University of Technology Sydney, Australia, where he is currently a Professor and the Head of the Discipline of Electrical Power and Energy Systems with the School of Electrical and Data Engineering. He has authored or coauthored more than 100 international journals and held two patents in power electronics. His current research interests include efficient, cost-effective, and reliable power conversion for renewable energy sources, energy storage systems, and microgrids. He is also serving as the Chair for the Joint Chapter IAS/IES/PELS (IEEE New South Wales Section) and an Associate Editor for the IEEE TRANSACTIONS ON INDUSTRIAL ELECTRONICS.
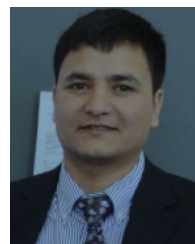
YAM P. SIWAKOTI (Senior Member, IEEE) received the B.Tech. degree in electrical engineering from the National Institute of Technology Hamirpur, Hamirpur, India, in 2005, the joint M.E. degree in electrical power engineering from the Norwegian University of Science and Technology, Trondheim, Norway, and Kathmandu University, Dhulikhel, Nepal, in 2010, and the Ph.D. degree in electronic engineering from Macquarie University, Sydney, Australia, in 2014. From 2014 to 2016, he was a Postdoctoral Fellow with the Department of Energy Technology, Aalborg University, Denmark. From 2017 to 2018, he was a Visiting Scientist with the Fraunhofer Institute for Solar Energy Systems, Freiburg, Germany. He is currently a Senior Lecturer with the Faculty of Engineering and Information Technology, University of Technology Sydney, Australia. He was a recipient of the prestigious Green Talent Award from the Federal Ministry of Education and Research, Germany, in 2016. He serves as an Associate Editor for three major journals of IEEE, namely IEEE TRANSACTIONS ON POWER ELECTRONICS, IEEE TRANSACTIONS ON INDUSTRIAL ELECTRONICS, IEEE JOURNAL OF EMERGING AND SELECTED TOPICS IN POWER ELECTRONICS, and the *IET Power Electronics*.

H. Aljarajreh *et al.*: Method of Seamless Transitions Between Different Operating Modes for Three-Port DC-DC Converters

IEEE *Access*

RICARDO P. AGUILERA (Member, IEEE) received the B.Sc. degree in electrical engineering from the Universidad de Antofagasta, Antofagasta, Chile, in 2003, the M.Sc. degree in electronics engineering from Universidad Técnica Federico Santa María, Valparaíso, Chile, in 2007, and the Ph.D. degree in electrical engineering from The University of Newcastle (UoN), Newcastle, NSW, Australia, in 2012. From 2012 to 2013, he was a Research Academic at UoN, where he was part of the Centre for Complex Dynamic Systems and Control. From 2014 to 2016, he was a Senior Research Associate at the University of New South Wales, Australia, where he was part of the Australian Energy Research Institute. Since September 2016, he has been with the School of Electrical and Data Engineering, University of Technology Sydney, Australia, where he is currently a Senior Lecturer. His main research interests include theoretical and practical aspects on model predictive control with application to power electronics, renewable energy integration, and microgrids.

CHI K. TSE (Fellow, IEEE) received the B.Eng. (Hons.) and Ph.D. degrees from the University of Melbourne, Melbourne, Australia, in 1987 and 1991, respectively. From 2005 to 2012, he was the Head of the Department of Electronic and Information Engineering, The Hong Kong Polytechnic University, Hong Kong. He is currently the Chair Professor of Electronic Engineering, The Hong Kong Polytechnic University, Hong Kong. He has been appointed to honorary professorship and distinguished fellowship by a few Australian, Canadian, and Chinese Universities, including the Chang Jiang Scholar Chair with the Huazhong University of Science and Technology and a Distinguished Professor-at-Large with the University of Western Australia. He is currently serving on panels of Hong Kong Research Grants Council, Innovation Technology Fund, and National Science Foundation of China. His research interests include complex network applications, power electronics, and nonlinear systems. He has served on a number of IEEE committees, including the IEEE Fellows Committee and the IEEE Awards Committee. He was a recipient of a number of research prizes, including a few Best Paper Prizes from IEEE and other journals, and two Gold Medals from the International Inventions Exhibition in Geneva and a Silver Medal from International Invention Innovation Competition in Canada. In 2006, he chaired the IEEE CAS Technical Committee on Nonlinear Circuits and Systems. He serves and has served as the Editor-in-Chief for IEEE TRANSACTIONS ON CIRCUITS AND SYSTEMS II, *IEEE Circuits and Systems Magazine*, an Editor for *IJCTA*, and an associate editor for a few other IEEE journals. In 2005 and 2010, he was selected as a IEEE Distinguished Lecturer.

● ● ●